

Regulation of superconductivity in Nb thin films induced by interstitial oxygen atoms

Yuchuan Liu(刘钰川), Ming Yang(杨明), Yun Fan(范云), Zulei Xu(徐祖磊), Yu Wu(吴禹), Yixin Liu(刘以鑫), Wei Peng(彭炜), Gang Mu(牟刚), and Zhi-Rong Lin(林志荣)

Citation: Chin. Phys. B, 2025, 34 (**4**): 047401. DOI: 10.1088/1674-1056/adb26c
Journal homepage: http://cpb.iphy.ac.cn; http://iopscience.iop.org/cpb

What follows is a list of articles you may be interested in

Intermediately coupled type-II superconductivity in a La-based kagome metal La_3Al

Yingpeng Yu(于英鹏), Zhaolong Liu(刘兆龙), Zhaoxu Chen(陈昭旭), Qi Li(李琦), Yulong Wang(王玉龙), Xuhui Wang(王旭辉), Chunsheng Gong(龚春生), Zhaotong Zhuang(庄照通), Bin-Bin Ruan(阮彬彬), Huifen Ren(任会芬), Peijie Sun(孙培杰), Jian-Gang Guo(郭建刚), and Shifeng Jin(金士锋)

Chin. Phys. B, 2025, 34 (**1**): 017401. DOI: 10.1088/1674-1056/ad8f9f

Multi-band analysis on physical properties of superconducting FeSe films

Jian-Tao Che(车剑韬) and Chen-Xiao Ye(叶晨骁)

Chin. Phys. B, 2023, 32 (**9**): 097401. DOI: 10.1088/1674-1056/acd3e5

Abnormal magnetoresistance effect in the Nb/Si superconductor-semiconductor heterojunction

Zhi-Wei Hu(胡志伟) and Xiang-Gang Qiu(邱祥冈)

Chin. Phys. B, 2023, 32 (**3**): 037401. DOI: 10.1088/1674-1056/ac8af7

Superconducting properties of the C15-type Laves phase $ZrIr_2$ with an Ir-based kagome lattice

Qing-Song Yang(杨清松), Bin-Bin Ruan(阮彬彬), Meng-Hu Zhou(周孟虎), Ya-Dong Gu(谷亚东), Ming-Wei Ma(马明伟), Gen-Fu Chen(陈根富), and Zhi-An Ren(任治安)

Chin. Phys. B, 2023, 32 (**1**): 017402. DOI: 10.1088/1674-1056/aca3a2

Fabrication and properties of the meander nanowires based on ultra-thin Nb films

Zhao Lu (赵璐), Jin Yi-Rong (金贻荣), Li Jie (李洁), Deng Hui (邓辉), Zheng Dong-Ning (郑东宁)

Chin. Phys. B, 2014, 23 (**8**): 087402. DOI: 10.1088/1674-1056/23/8/087402

Regulation of superconductivity in Nb thin films induced by interstitial oxygen atoms

Yuchuan Liu(刘钰川)[1,2], Ming Yang(杨明)[1,2], Yun Fan(范云)[1,2], Zulei Xu(徐祖磊)[2,3], Yu Wu(吴禹)[2], Yixin Liu(刘以鑫)[2,3], Wei Peng(彭炜)[2,3], Gang Mu(牟刚)[2,3,†], and Zhi-Rong Lin(林志荣)[1,2,3,‡]

[1] *Shanghai University, Shanghai* 200444, *China*
[2] *State Key Laboratory of Materials for Integrated Circuits, Shanghai Institute of Microsystem and Information Technology, Chinese Academy of Sciences, Shanghai* 200050, *China*
[3] *University of Chinese Academy of Sciences, Beijing* 100049, *China*

(Received 12 December 2024; revised manuscript received 14 January 2025; accepted manuscript online 5 February 2025)

The regulation of superconductivity in thin films can provide important information on low-dimensional superconducting properties, and also has important reference values for the application in superconducting devices. Herein, we report the successful regulation of both the superconductivity and normal-state properties of Nb films in a wide range by the controllable introduction of interstitial oxygen atoms. The lattice parameter is enhanced for an extent as large as 4.4%, and the normal-state resistivity ρ_n is tuned for more than 15 times. The slope of upper critical field near T_c shows a close correlation with ρ_n in a wide range. Importantly, it is found that the suppression of T_c by disorder reveals a linear dependence with ρ_n in the region with an unchanged crystalline quality, which can be understood based on the picture of three-dimensional ballistic motion.

Keywords: Nb film, regulation of superconductivity, upper critical field

PACS: 74.70.–b, 74.78.–w, 74.25.Op, 74.62.Bf

DOI: 10.1088/1674-1056/adb26c **CSTR:** 32038.14.CPB.adb26c

1. Introduction

Due to the enhancement of fluctuation effect and the weakening of Coulomb shielding caused by dimensional effect, the response of superconductivity to external conditions in superconducting (SC) thin film systems is an important subject.[1–3] Disorder is one of the important factors to regulate superconductivity.[4–6] Superconductivity can be suppressed by disorder in terms of weakening the attractive interaction leading to Cooper pairing (the fermionic scenario)[2,7] or destroying long-range order of the macroscopic phase (the bosonic scenario).[2,8] It is the latter case that is noteworthy, since it implies the loss of superconductivity in the presence of electron pairs. In fact, in terms of physical nature, it is closely related to the model of pre-formed Cooper pairs that has been proposed in copper-based high-temperature superconductors.[9] Even within the fermionic scenario, the suppression of superconductivity by disorder at the three-dimensional (3D) and two-dimensional (2D) limits also exhibits significant differences. Meanwhile, the contribution of electron diffusion and ballistic motion to the suppression of T_c also varies.[10]

Benefitting from the high critical transition temperature T_c, stable chemical properties and excellent machinability, niobium (Nb) film has become one of the basic materials for the manufacture of advanced SC electronic devices.[11–15] As the thickness of the film decreases, the dimensional effect on the value of T_c and the degree of disorder gradually becomes prominent.[16,17] In addition, the method of ion implantation was used to tune the disorder level, thus regulating the SC and normal-state properties of Nb films.[18] Also, it was found that the introduction of interstitial oxygen atoms can directly regulate the disorder of bulk Nb material.[19] Although the effect of oxidation or the oxygen diffusion on Nb films has also been noticed,[20–22] a systematic investigation on the performance of Nb films under the effect of interstitial oxygen atoms is still lacking.

In this work, we supply a route to tune the superconductivity by the controllable introduction of interstitial oxygen atoms to the Nb films. Both the SC transition temperature T_c and the normal-state resistivity ρ_n are regulated in a wide range: T_c is suppressed from 9.2 K to 0 K while ρ_n is enhanced by more than 15 times. Meanwhile, the slope of upper critical field near T_c is also regulated by the disorder, revealing a linear dependence with ρ_n. A further analysis shows that the evolution of T_c with disorder is in accord with the physical picture of 3D ballistic motion. Since the diffusion of a small amount of oxygen atoms is inevitable on the surface of Nb film or at the interface between it and the oxide substrate, the result of this study is also of great value for the application of Nb films in SC devices.

†Corresponding author. E-mail: mugang@mail.sim.ac.cn
‡Corresponding author. E-mail: zrlin@mail.sim.ac.cn

© 2025 Chinese Physical Society and IOP Publishing Ltd. All rights, including for text and data mining, AI training, and similar technologies, are reserved.

2. Materials and methods

Direct current (DC) reactive magnetron sputtering was utilized to deposit the Nb film onto a 2-inch (1 inch = 2.54 cm) high-resistance silicon (Si) substrate. The reaction chamber is equipped with a high-purity Nb target (99.99%) and maintains a vacuum of approximately 10^{-8} Pa. During the sputtering process, the flow rate of argon gas, the chamber pressure, and the sputtering power were set to 20 sccm, 0.2 Pa, and 150 W, respectively. These conditions facilitated the production of high-quality Nb films. Furthermore, adjusting the magnetron sputtering time allows for the precise controlling of the film thickness to around 150 nm. Silicon wafers were cut into small pieces with the size of 5 cm×5 cm after magnetron sputtering, then divided into multiple groups to carry out the following experiments.

The small samples were placed in a tube furnace for thermal treatment under various conditions. Prior to the treatment, the tube furnace was purged by high-pure Ar gas for 60 minutes to eliminate any residual air. The samples were annealed in the inert gas under different temperatures. Very similar results were obtained between the treatments under pure Ar gas and Ar/N_2 mixture (with the ratio Ar:N_2 = 9:1). Unless otherwise indicated, the results reported herein are based on treatments under the mixed atmosphere. The treating time was fixed to 40 minutes for all the samples.

The crystal structure of films was measured by x-ray diffraction (XRD, HaoYuan DX-2700). The element contents were measured using the time-of-flight secondary ion mass spectrometry (ION-TOF GmbH, TOF-SIMS 5-100). The surface morphologies of films were measured by atomic force microscope (AFM, Bruker Dimension Icon) and scanning electron microscopy (SEM, Zeiss Gemini300). The electrical transport measurements were performed using the standard four-wire method in a physical property measurement system (PPMS, Quantum Design) with the magnetic field of up to 9 T. The magnetic field were applied vertical to the film surface.

3. Results

3.1. Characterization

The crystal structure of the Nb films with different treating temperature (T_{tr}) was checked by XRD, see Fig. 1(a). For the untreated pristine sample, the clear diffraction peak can been seen at around 38.8°, which is assigned to the (110) diffraction peak of Nb with a space group of *Im*-3*m*. The peak position of the untreated Nb film is about 0.2° higher than that of the bulk Nb (see the black symbols in Fig. 1(a)). In addition, the full width at half maximum (FWHM) of the Nb film (∼ 0.50°) is several times larger than the bulk sample (∼ 0.17°). With the increase of T_{tr}, the position of this peak shifts to the left side gradually, indicating the expansion of the crystal lattice. In the situations with T_{tr} below 260 °C, the intensity of the (110) peak is enhanced as compared with the untreated sample. Meanwhile, the value of FWHM is reduced to about 0.41°. These experimental facts indicate that low-temperature treatment has an improving effect on the crystalline of quality Nb films. The values of lattice parameter of the samples were calculated by using the Bragg's Law ($2d\sin\theta = n\lambda$), which are shown in Fig. 1(b). The lattice parameter a increases from 3.284 Å to 3.427 Å as T_{tr} increases to 350 °C, which is equivalent to a change of up to 4.4%. It is worth pointing out that this is a large magnitude of expansion, which is several times larger than that reported in bulk Nb samples.[19] And the lattice parameter of some samples has reached or even exceeded the value of Ta film (∼ 3.32 Å) with the same structure.[23]

In order to obtain further information about the interior of the sample, we examined the depth-resolved element content of the pristine and treated samples by means of time-of-flight secondary ion mass spectrometry (TOF-SIMS). The information at different depth of the films was collected by etching the samples controllably using cesium ions with the energy of 1 keV. As shown in Fig. 1(c), in the vicinity of the film surface, oxygen element shows the high intensity. This is due to the fact that the Nb film naturally oxidizes to form an oxide layer when it is exposed to air. The increase of the intensity when the depth is larger than 150 nm comes from the SiO_2 layer on the substrate, which is formed by natural oxidation of Si substrate upon exposure to air. A clear trend is that the intensity of the oxygen element inside the film shows a significant increase as the treating temperature increases. Considering the fact that the crystal structure remains unchanged as evidenced by the XRD data in Fig. 1(a), we argue that the heat treatment allows oxygen atoms to diffuse into the Nb film and exist as interstitial atoms.[24] The presence of interstitial oxygen atoms leads to the increase in the lattice parameter of the Nb films, see Fig. 1(d).

The surface morphology of the films was measured by AFM. Here we show the AFM image of the sample with T_{tr} = 200 °C in Fig. 1(e) as an example. The root-mean-square roughness is about 0.9 nm, indicating a high level of flatness. In addition, we used a scanning electron microscope to observe the surface topography of the pristine and treated Nb films at a magnification of 5×10^4, see Figs. 1(f) and 1(g). Both the AFM and SEM images reveal the smooth and dense surface of the Nb film. The elongated grain shape can be observed in the SEM image on both the pristine and treated samples, indicating that the treatment process does not change the surface morphology of the films. In addition, no trace of nitrogen element was detected in the treated samples by both the energy dispersive x-ray spectroscopy and TOF-SIMS measurements. This indicates that despite the presence of N_2 in the atmosphere of the heat treatment, the nitrogen element does not enter the interior of the sample at mild temperatures below 350 °C.

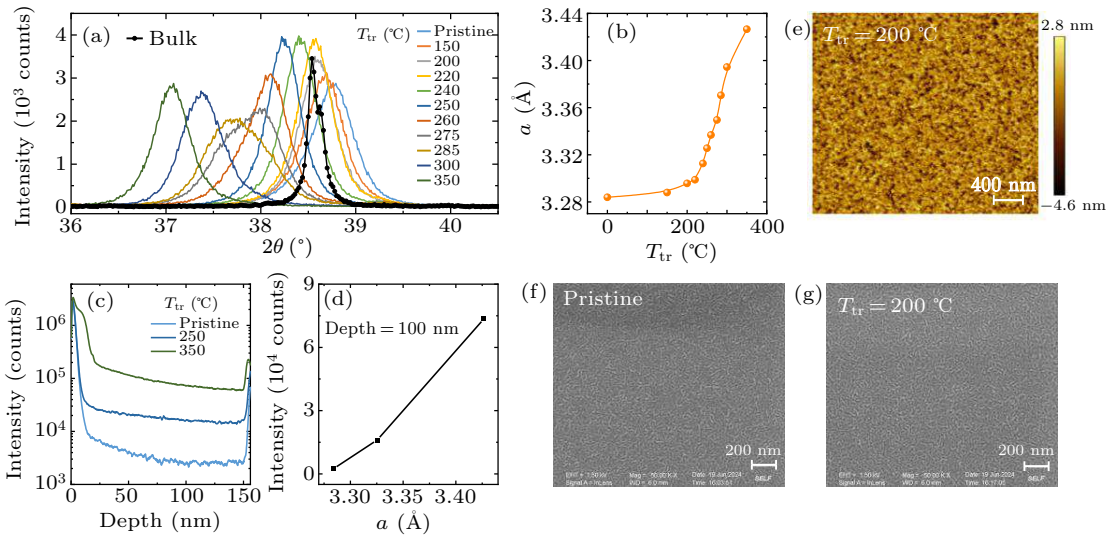


Fig. 1. (a) XRD patterns of the Nb films with different treating temperatures. The data of bulk sample is also shown for a comparison. (b) Lattice parameter a as a function of the treating temperature T_{tr}. (c) The intensity of oxygen element from the TOF-SIMS measurement as a function of the depth for the three Nb samples with different T_{tr} treated under Ar atmosphere. (d) The intensity of oxygen element in the TOF-SIMS at the depth of 100 nm as a function of the lattice parameter. (e) AFM images of the Nb sample with $T_{tr} = 200$ °C. (f) SEM picture of the pristine Nb sample. (g) SEM picture of the Nb sample with $T_{tr} = 200$ °C.

3.2. Superconducting and normal-state properties

The electrical transport measurements were carried out to study the physical properties of the samples annealed at different temperatures in both the superconducting and normal states. In Fig. 2(a), we show the temperature dependent resistivity of Nb films treated at different temperature. Clear SC transitions can be observed in the low-temperature region. All the samples reveal a metallic behavior in the normal state above the SC critical temperature T_c. Meanwhile, the magnitudes of resistivity ρ in the normal-state show a systematical increase with T_{tr}. In order to unveil the evolution tendency of ρ with temperature, we display the normalized resistivity $\rho/\rho_{300\ K}$ in Fig. 2(b). It is clear that the residual value of $\rho/\rho_{300\ K}$ at low temperature is enhanced systematically when the the value of T_{tr} is increased. Thus, the residual resistance ratio, RRR = $\rho_{300\ K}/\rho_n$ (ρ_n is the normal-state resistivity at temperature just above T_c), will reveal an decreasing evolutionary trend with T_{tr}. The SC transition can be seen more clearly in Fig. 2(c). The pristine sample shows the T_c of 9.2 K (50% ρ_n), which is consistent with the bulk material.[19] It is found that the SC critical temperature T_c reveals a systematical decrease with the increase of T_{tr}. Superconductivity vanishes in the temperature range above 2 K when T_{tr} is raised to 350 °C.

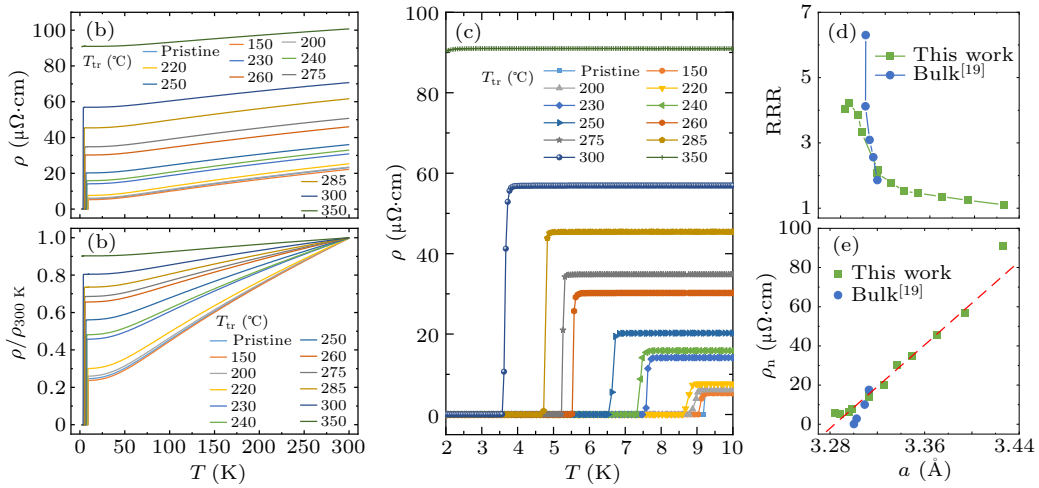


Fig. 2. (a) Temperature dependence of resistivity ρ under zero field for Nb films with different T_{tr}. (b) The resistivity data normalized to the values at 300 K. (c) An enlarged view of the ρ–T data in the low temperature range below 10 K. (d)–(e) The residual resistance ratio and normal-state resistivity as a function of the lattice parameter. The results of bulk Nb samples are also shown for a comparison.[19] The red dashed line in (e) is the guide for eyes.

In order to unveil the correlation between the physical properties and crystal structure, we plot RRR and ρ_n as a function of lattice parameter a in Figs. 2(d) and 2(e). The data of the bulk samples are also shown for a comparison.[19] RRR reveals a slight increase (corresponding to $T_{tr} \leq 150$ °C) and then declines monotonically with the enhancement of a. ρ_n exhibits a roughly opposite evolutionary trend compared to RRR. This result indicates that as a increases, which reflects an in-

crease in the amount of interstitial oxygen atoms in the Nb film, the degree of disorder gradually increases. The slight increase (decrease) in RRR (ρ_n) of the sample treated at 150 °C is likely due to the improvement of the film crystalline quality by annealing treatment, which can be reflected in the increase (decrease) of the XRD intensity (FWHM) (see Fig. 1(a)). Furthermore, we noticed that compared to bulk material, the evolution trend of RRR and ρ_n with a is relatively more gentle in Nb thin films.

3.3. Upper critical field

The behaviors of electrical transport under external magnetic field were measured to study the field-induced pair-breaking effect. In Figs. 3(a)–3(c), we show temperature-dependent resistivity under various magnetic fields for the samples under three typical values of T_{tr}. It is clear that, as the magnetic field increases, the SC transition shifts to lower temperatures for all the three samples. The temperature dependence of upper critical field $\mu_0 H_{c2}$ for all the eleven samples is shown in Fig. 3(d). The criteria of 50%ρ_n is adopted in determining the values of $\mu_0 H_{c2}$.

All the samples show the roughly linear tendency in the $\mu_0 H_{c2}$–T curves. The slope of the upper critical field reveals a clear enhancement with the decrease of T_c. To have a quantitative comparison, we calculate and plot this slope, $-\mathrm{d}\mu_0 H_{c2}(T)/\mathrm{d}T|_{T_c}$, as a function of ρ_n in Fig. 3(e). $-\mathrm{d}\mu_0 H_{c2}(T)/\mathrm{d}T|_{T_c}$ and ρ_n exhibit a positive correlation and a linear trend over a wide range, as shown by the red dashed line. This evolution tendency is in accord with the empirical law[25] that, in the dirty limit, the value of $-\mathrm{d}\mu_0 H_{c2}(T)/\mathrm{d}T|_{T_c}$ is proportional to ρ_n if the normal-state electronic specific heat coefficient γ_n has no much change. Similar behavior has been reported in other SC films like NbN[26] and TiN.[27]

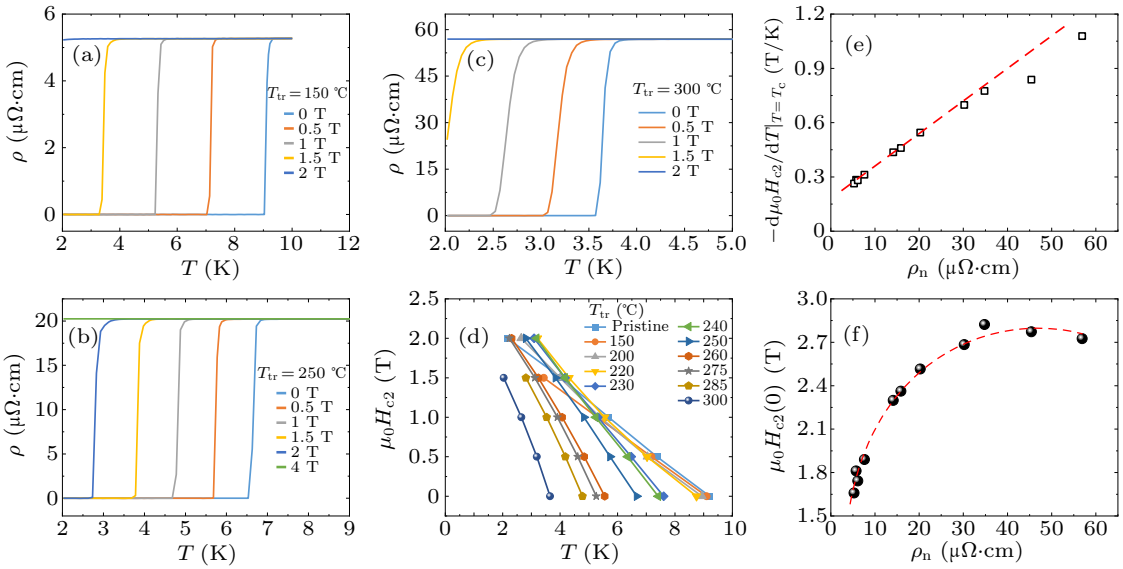


Fig. 3. (a)–(c) Temperature-dependent resistivity in different vertical magnetic fields for the three films with T_{tr} = 150 °C (a), 250 °C (b), and 300 °C (c). (d) Upper critical field $\mu_0 H_{c2}$ versus temperature for Nb films with different T_{tr}. (e) The slope of upper critical field, $-\mathrm{d}\mu_0 H_{c2}/\mathrm{d}T|_{T_c}$, as a function of ρ_n. (f) The zero-temperature upper critical field $\mu_0 H_{c2}(0)$ as a function of ρ_n. The red dashed lines are guide for eyes.

Using the Werthamer–Helfand–Hohenberg relation,[28] $\mu_0 H_{c2}(0) = -0.693 \times \mathrm{d}\mu_0 H_{c2}(T)/\mathrm{d}T|_{T_c} \times T_c$, the zero-temperature upper critical field $\mu_0 H_{c2}(0)$ is determined, which is shown in Fig. 3(f). It can be seen that, in a wide region, the value of $\mu_0 H_{c2}(0)$ reveals an increasing tendency with the increase of ρ_n, which can be attributed to the enhancement of $-\mathrm{d}\mu_0 H_{c2}(T)/\mathrm{d}T|_{T_c}$ with ρ_n.

4. Discussion

We first discuss the diffusion of oxygen atoms in Nb films. In fact, this issue has been studied very early based on bulk Nb material and important information such as diffusion coefficient has been obtained.[29] In addition, it was found that, in the temperature range of 250 °C–380 °C, the decomposition of niobium oxide on the surface supplies oxygen source, which diffuses deeply into the depths of Nb material with a diffusion coefficient that increases with baking temperature.[30] It is notable that, in the previous study, the content of oxygen source is limited due to the removal of the oxide layer on the sample surface by the electropolishing (EP) treatment. The small amount of oxygen source comes from short-term exposure to air after EP treatment. In this case, the concentration of oxygen atoms in the depths was found to decrease with the increase of treating temperature,[30] which is different from the present result (see Fig. 1(c)). In our work, the Nb films were not polished, leaving relatively greater amount of oxide layer on the surface. This provides a more sufficient oxygen source for subsequent heat treatment. Thus, the samples treated at higher temperatures reveal a higher level of oxygen concentration. Roughly speaking, the amount of oxygen source de-

pends on the thickness of the oxide layer on the surface of the Nb film. The latter is mainly determined by the exposure time to air,[31] which is about half an hour in our experiment. Moreover, in agreement with previous report,[30] our result also indicates that treating temperature is the main factor affecting the diffusion of oxygen atoms inside the Nb material.

The evolution of superconductivity under the influence of disorder is another important issue that has attracted widespread attention. As we have mentioned, disorder mainly destroys superconductivity by suppressing the pairing strength of SC Cooper pairs.[7] At the same time, the localization effect caused by disorder may also lead to a decrease in the density of states at the Fermi level, thereby weakening the superconductivity. In SC thin films, due to the accentuation of fluctuation effect, another mechanism for suppressing superconductivity may become important. Disorder can disrupt superconductivity by destroying the long-range coherence of the phase of Cooper pairs.[8] In the phase-driven pathway, typically the breakdown of superconductivity is accompanied by an enhancement of the sheet resistance to resistance quantum $R_q = 6.5$ kΩ.[3] An estimation shows that the maximum sheet resistance of our samples is about 3.8 Ω, which is much smaller than R_q. This rules out the possibility for the phase-driven scenario.

To catch more details concerning the disorder-induced suppression of superconductivity, we display the data of T_c as a function of ρ_n in Fig. 4(a). Actually here ρ_n serves as an evaluation of the disorder level since it contains the information about the scattering relaxation time of electrons. It can be seen that T_c reveals a linear evolution with ρ_n in the low ρ_n range ($\rho_n < 25$ μΩ·cm), see the shadow area in Fig. 4. We note that the departure from this linear tendency in the high ρ_n region is accompanied by the decreasing of the x-ray diffraction intensity of the (110) peak which actually reflects the crystalline quality of Nb film, see Fig. 4(b). This suggests that although the introduction of interstitial oxygen atoms and the degradation in crystalline quality both cause an enhancement of ρ_n, these two factors have different effects on superconductivity. This is a point that requires extra attention in the analysis of disorder induced suppresion of superconductivity. Thus, it is clear that a simple relation

$$T_c = T_{c0}(1 - A\rho_n) \tag{1}$$

is obeyed, provided that the crystalline quality of the film remains unchanged. Here A and T_{c0} are fitting parameters. The data in the low ρ_n region ($\rho_n < 25$ μΩ·cm) is fitted using Eq. (1), see the red dashed lines in Fig. 4(a). The fitting curve shows a rather fine description to the experimental data. The resultant parameters are summarized in Table 1. The data of the bulk samples also follow this linear relation. Surprisingly, despite the obviously different values of ρ_n with the same T_c, the value of AT_{c0} of the bulk material is almost identical to that of the thin film. This reflects the intrinsic behavior of Nb materials in terms of the suppression rate of superconductivity under the influence of disorder.

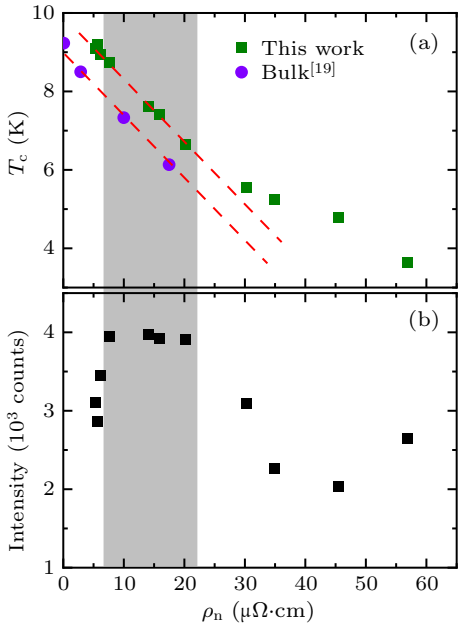


Fig. 4. (a) T_c as a function of ρ_n. The data of bulk samples[19] is also shown for a comparison. The red dashed lines are the fitting results using Eq. (1). (b) XRD intensity of the (110) peak as a function of ρ_n.

Table 1. Fitting parameters of film and bulk Nb materials using Eq. (1).

Status	T_{c0} (K)	A (μΩ·cm)$^{-1}$	AT_{c0} K/(μΩ·cm)	Ref.
Film	9.95	0.0163	0.162	this work
Bulk	8.96	0.0181	0.162	[19]

Actually, the evolutionary behavior of T_c with ρ_n can be explained within the framework of 3D ballistic electron motion.[10] In general, the presence of disorder can cause the scattering on Friedel oscillations and enhance the electron–electron repulsion and the Coulomb pseudo-potential, which leads to the suppression of the effective electron–phonon coupling constant λ. It was pointed out that,[10,32] in the 3D geometry, the diffusive contributions can be extended to the ballistic region in the system with weak localization. As a result, the correction to λ mainly comes from small scales with the order of the Fermi wavelength and the suppression of superconductivity by disorder is controlled by the parameter $k_F l$,[10]

$$T_c = T_{c0}(1 - \alpha/k_F l). \tag{2}$$

Here k_F and l are the Fermi momentum and the mean free path of electrons respectively. On the other hand, based on the Drude model, the normal-state resistivity can be expressed as

$$\rho_n = (\hbar k_F^2/nq^2)(1/k_F l), \tag{3}$$

assuming a spherical Fermi surface. Here $\hbar$, n, and q are the Planck constant, charge carrier density, and charge of an electron, respectively. It follows that the normal-state resistivity

ρ_n is proportional to $1/(k_F l)$ in the case where the disorder induced changes in l dominate. In this sense, equations (1) and (2) are equivalent. This is rather different from the 3D diffusive scenario, where a $1/(k_F l)^2$ dependence of the T_c correction should be obeyed.[10] Thus, the behavior of the T_c evolution shown in Fig. 4(a) is in accordance with what is expected from the mechanism of 3D ballistics.[10]

It is worth pointing out that the process of introducing disorder in the Nb film may not be as simple as interstitial oxygen atoms acting as scattering centers. It has been known that in Nb materials, interstitial oxygen atoms predominantly occupy the octahedral sites of the body centered cubic lattice, which leads to the lattice distortions in the local neighborhood.[33,34] The distorted region, as a whole, may act as the scattering centers in practice.

5. Conclusions

In summary, we studied the regulation of superconductivity in Nb thin films by the introduction of interstitial oxygen atoms. The expansion of lattice parameter induced by the injection of oxygen atoms can be as high as 4.4%, clearly larger than that reported in bulk samples. The residual resistance ratio RRR, normal-state resistivity ρ_n, and the slope of upper critical field $-\mathrm{d}\mu_0 H_{c2}(T)/\mathrm{d}T|_{T_c}$ all reveal the systematical evolution with the increase of annealing temperature. Notably, the suppression of T_c by the disorder induced by interstitial oxygen atoms displays a linear dependence with ρ_n, which is consistent with the expectation from the mechanism of 3D ballistics.

Acknowledgements

Project supported by the Strategic Priority Research Program of the Chinese Academy of Sciences (Grant No. XDB0670000), the National Key Research and Development Program of China (Grant No. 2023YFB4404904), the Key-Area Research and Development Program of Guangdong Province, China (Grant No. 2020B0303030002), and the Autonomous Deployment Project of State Key Laboratory of Materials for Integrated Circuits (Grant No. SKLJC-Z2024-B04). The authors would like to thank all the staff at the Superconducting Electronics Facility (SELF) for their assistance.

References

[1] Sondhi S L, Girvin S M, Carini J P and Shahar D 1997 *Rev. Mod. Phys.* **69** 315
[2] Wang Z, Liu Y, Ji C and Wang J 2023 *Rep. Prog. Phys.* **87** 014502
[3] Sacépé B, Feigel'man M and Klapwijk T M 2020 *Nat. Phys.* **16** 734
[4] Anderson P W, Muttalib K A and Ramakrishnan T V 1983 *Phys. Rev. B* **28** 117
[5] Sacépé B, Chapelier C, Baturina T I, Vinokur V M, Baklanov M R and Sanquer M 2008 *Phys. Rev. Lett.* **101** 157006
[6] Wang T, Yu A, Mao Y, *et al*. 2023 *Supercond. Sci. Technol.* **36** 125015
[7] Finkel'stein A 1994 *Physica B* **197** 636
[8] Fisher M P A 1990 *Phys. Rev. Lett.* **65** 923
[9] Božović I and Levy J 2020 *Nat. Phys.* **16** 712
[10] Antonenko D S and Skvortsov M A 2020 *JETP Lett.* **112** 428
[11] Russo R, Granata C, Vettoliere A, Esposito E, Fretto M, Leo N D, Enrico E and Lacquaniti V 2014 *Supercond. Sci. Technol.* **27** 044028
[12] Karasik B S, Gaidis M C, McGrath W R, Bumble B and LeDuc H G 1997 *Appl. Phys. Lett.* **71** 1567
[13] Wang Y, Chen L, Pan Y, *et al*. 2023 *ACS Nano* **17** 15466
[14] Duan S, Wu J, Fan K, Zhang C, Jin B, Chen J and Wu P 2022 *J. Funct. Mater. Dev.* **28** 7 (in Chinese)
[15] Zhang L, Xu Z, Li X, *et al*. 2023 *Chin. Phys. B* **32** 047302
[16] Minhaj M S M, Meepagala S, Chen J T and Wenger L E 1994 *Phys. Rev. B* **49** 15235
[17] Pinto N, Rezvani S J, Perali A, Flammia L, Milošević M V, Fretto M, Cassiago C and Leo N D 2018 *Sci. Rep.* **8** 4710
[18] Camerlingo C, Scardi P, Tosello C and Vaglio R 1985 *Phys. Rev. B* **31** 3121
[19] Koch C C, Scarbrough J O and Kroeger D M 1974 *Phys. Rev. B* **9** 888
[20] Lacquaniti V, Maggi S, Monticone E and Steni R 1993 *Appl. Supercond.* **1** 845
[21] Henry M D, Wolfley S, Young T, Monson T, Pearce C J, Lewis R, Clark B, Brunke L and Missert N 2017 *IEEE Trans. Appl. Supercond.* **27** 1100505
[22] Wang L, Zhong Y, Li J, Cao W, Zhong Q, Wang X and Li X 2018 *Mater. Res. Express* **5** 046410
[23] Liu Y, Zhang H, Han X, *et al*. 2022 *Supercond. Sci. Technol.* **35** 055010
[24] Straumanis M E and Zyszczynski S 1970 *J. Appl. Cryst.* **3** 1
[25] Jaffe J E 1989 *Phys. Rev. B* **40** 2558
[26] Wang X, Wang L, Liu Y, Gao W, Wu Y, Xu Z, Jin H, Zhang L, Peng W, Wang Z, Li W, Mu G and Lin Z 2023 *Physica C* **606** 1354223
[27] Liu Y X, Liu Y C, Xu Z, Yu A, Wang X, Peng W, Wu Y, Mu G and Lin Z 2024 *Supercond. Sci. Technol.* **37** 105015
[28] Werthamer N R, Helfand E and Hohenberg P C 1966 *Phys. Rev.* **147** 295
[29] Boratto F J M and Reed-Hill R E 1977 *Metall. Trans. A* **8** 1233
[30] Yu M, Huang S, Zhao Y, *et al*. 2024 *Supercond. Sci. Technol.* **37** 105014
[31] Verjauw J, Potočnik A, Mongillo M, *et al*. 2021 *Phys. Rev. Appl.* **16** 014018
[32] Adams P W, Browne D A and Paalanen M A 1992 *Phys. Rev. B* **45** 8837
[33] Dosch H, Schwerin A V and Peisl J 1986 *Phys. Rev. B* **34** 1654
[34] Delheusy M, Stierle A, Kasper N, Kurta R P, Vlad A, Dosch H, Antoine C, Resta A, Lundgren E and Andersen J 2008 *Appl. Phys. Lett.* **92** 101911